phys. stat. sol. (b) **209**, 413 (1998)

Subject classification: 74.25.Fy; 74.25.Jb; 74.72.Bk; S10.15

Thermal Transport in 90 K- and 60 K-Phase $YBa_2Cu_3O_{7-\delta}$ High-T_c Oxides

M. IKEBE (a), H. FUJISHIRO (a), K. NAKASATO[1]) (a), T. MIKAMI (a), T. NAITO (b), and T. FUKASE (b)

(a) Department of Materials Science and Technology, Faculty of Engineering, Iwate University, 4-3-5 Ueda, Morioka 020-8551, Japan
e-mail address: ikebe@iwate-u.ac.jp; Fax: +81-19-621-6373, Tel.: +81-19-621-6362

(b) Institute for Materials Research, Tohoku University, 2-1-1 Katahira, Sendai 980-8577, Japan

(Received April 9, 1998; in revised form July 20, 1998)

The thermal diffusivity α and conductivity $\varkappa$ of $YBa_2Cu_3O_{7-\delta}$ sintered crystals with oxygen deficiencies $\delta \approx 0.10$ (90 K-phase) and $\delta \approx 0.35$ (60 K-phase) have been quasi-simultaneously measured between 15 and 170 K. The phonon and electron components of α and $\varkappa$ are separated and analyzed from viewpoints of both the d- and s-wave superconducting energy gap models. It is found that the enhancement of $\varkappa$ below T_c, which is commonly observed for 90 K- and 60 K-phase $YBa_2Cu_3O_{7-\delta}$, is consistent only with the phonon origin model under d-wave energy gap anisotropy with the maximum gap $2\Delta_{max}/k_B T_c \approx 5$. The phonon scattering mechanisms are synthetically analyzed for both 90 K- and 60 K-phase $YBa_2Cu_3O_{7-\delta}$ and the oxygen vacancy is found to be one of the dominant phonon scattering centers in this system.

1. Introduction

The thermal conduction is an important transport phenomenon in solids ranking with the electrical conduction. From the viewpoint of material physics, the thermal conduction is often more versatile than the electrical one because the former provides us with valuable information not only of conductors but also of insulators and even of superconductors below T_c. Thermal conductivity measurement, however, is far less popular than electrical resistivity measurement. It is desirable to accumulate the data of the thermal conductivity of various materials and to establish a standard method to analyze the thermal conductivity.

Recently, we have developed a quasi-simultaneous measuring system of the thermal diffusivity α and thermal conductivity $\varkappa$ under identical experimental set-ups [1, 2]. Because the diffusivity α is given by $\varkappa/C$, i.e., $\varkappa$ divided by the specific heat C, we can *'in situ'* determine the specific heat by measuring both α and $\varkappa$. To monitor the correct value of the Debye temperature Θ_D of the sample from the data of the specific heat enhances the reliability of analyses on the phonon thermal conductivity. In this paper we apply the α and $\varkappa$ simultaneously measuring method to 90 K- and 60 K-phase $YBa_2Cu_3O_{7-\delta}$ (YBCO) high-T_c superconductors and develop synthetic and self-consistent analyses for the thermal conductivity and diffusivity.

[1]) Present address: Shibaura Engineering Works Co. Ltd., 6-25-22 Sagamigaoka, Zama 228, Japan.

In the superconducting state, both the phonon component $\varkappa_{ph}(T)$ and electron component $\varkappa_e(T)$ of the thermal conductivity are determined intrinsically by the quasi-particle density $n_{qp}(T)$. Then $n_{qp}(T)$ is determined by the magnitude and the distribution of the energy gap $\Delta(T)$. Accordingly, the thermal conductivity can become a useful tool to determine the gap symmetry, or more precisely, the distribution of $\Delta(T)$ in a superconductor. We can expect to obtain useful information on the energy gap symmetry from the analyses of the thermal conductivity and diffusivity.

2. Experimental

$YBa_2Cu_3O_{7-\delta}$ polycrystals were prepared by a standard solid state reaction method. The stoichiometric mixtures of Y_2O_3, $BaCO_3$ and CuO powders were calcined at 910 °C for 24 h in air. They were pulverized, pressed into pellets, sintered at 955 °C for 30 h in flowing oxygen and then slowly cooled to room temperature in about 24 h. These samples were named as 90 K-YBCO. The 60 K-phase (60 K-YBCO) and non-superconductive samples were obtained by quenching the 90 K-YBCO into liquid nitrogen from 600 and 900 °C, respectively. The amount of the oxygen deficiency δ was determined to be $\delta = 0.10 \pm 0.01$ for 90 K-YBCO, 0.35 ± 0.01 for 60 K-YBCO and 0.75 ± 0.01 for non-superconductive YBCO by iodometric titration. The thermal conductivity was measured by a standard continuous heat flow method and the diffusivity was measured by an arbitrary heating method between 15 and 170 K. A Gifford-McMahon cycle helium refrigerator was used as a cryostat and AuFe(0.07 at%)–chromel thermocouples were used as thermometers. The measurement of the heat transport was performed automatically and details of the measuring system were described elsewhere [1, 2]. The phonon velocities in the present specimens were measured by a pulse superposition method using ≈ 7 MHz longitudinal and transverse ultrasound. The densities of the samples were determined by measuring the volume and weight, which were confirmed to be more than 90% of theoretical values. The grain sizes of the specimens were observed by use of a scanning electron microscope (SEM).

3. Experimental Results

Fig. 1 shows the temperature dependence of the electrical resistivity $\varrho(T)$ of the present 90 K-, 60 K- and non-superconductive YBCO samples. Both 90 K- and 60 K-YBCO show sharp superconducting transitions at $T_c = 92$ K and 62 K. The absolute values of $\varrho(T)$ of these samples are pretty small for sintered materials. But in comparison with good single crystals, the resistivity is large due to sizable residual resistivity $\varrho(0)$. In this sense the present sintered samples may be regarded as 'dirty' $YBa_2Cu_3O_{7-\delta}$. The $\varrho(T)$ curve of 90 K-YBCO follows the linear T law, while $\varrho(T)$ of 60 K-YBCO below about 200 K shows somewhat steeper reduction than T linear. These characteristics of $\varrho(T)$ are similar to those of single crystals [3, 4]. On the other hand, $\varrho(T)$ of non-superconductive YBCO shows semiconductive characteristics and $\varrho(T)$ increases with decreasing temperature below 170 K.

Fig. 2 shows the temperature dependence of the thermal conductivity $\varkappa(T)$ of the same samples as in Fig. 1. With decreasing temperature down to T_c, $\varkappa(T)$ of 90 K-YBCO slightly increases and then shows a characteristics enhancement related to the onset of superconductivity. $\varkappa(T)$ of 60 K-YBCO follows a qualitatively similar curve as that of 90 K-YBCO. The characteristic enhancement below T_c is, however, more con-

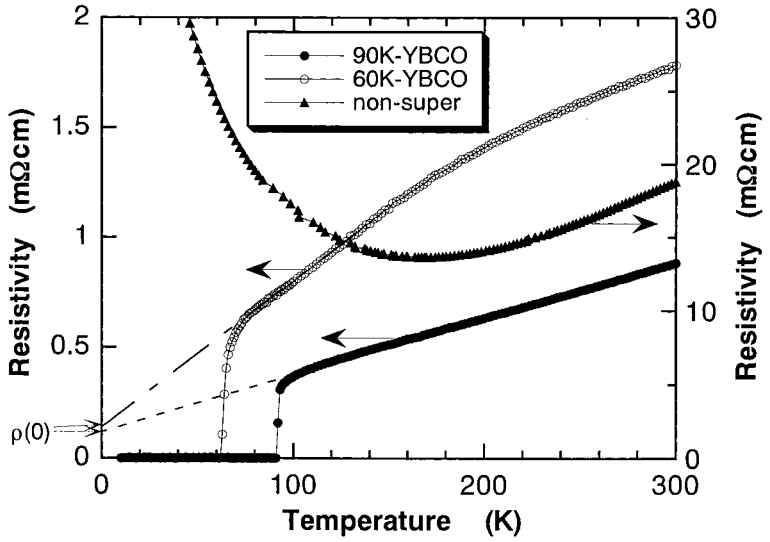

Fig. 1. $\varrho(T)$ vs. T for 90 K-, 60 K- and non-superconductive YBCO. The residual resistivity $\varrho(0)$ is obtained by linearly extrapolating ϱ to 0 K. The resistivity ratio $\varrho(T)/\varrho(0)$ is estimated to be 2.7 for 90 K-YBCO and 3.6 for 60 K-YBCO. $\varrho(T)$ of non-superconductive YBCO is also shown for comparison

spicuous for the 90 K-sample than for the 60 K-sample. $\varkappa(T)$ takes a maximum at $T_{max} \approx 45$ K for 90 K-YBCO and at $T_{max} \approx 37$ K for 60 K-YBCO. The absolute values of $\varkappa(T)$ of 60 K-YBCO are smaller than those of 90 K-YBCO over the entire measured temperature range. $\varkappa(T)$ of the non-superconductive sample is the smallest and de-

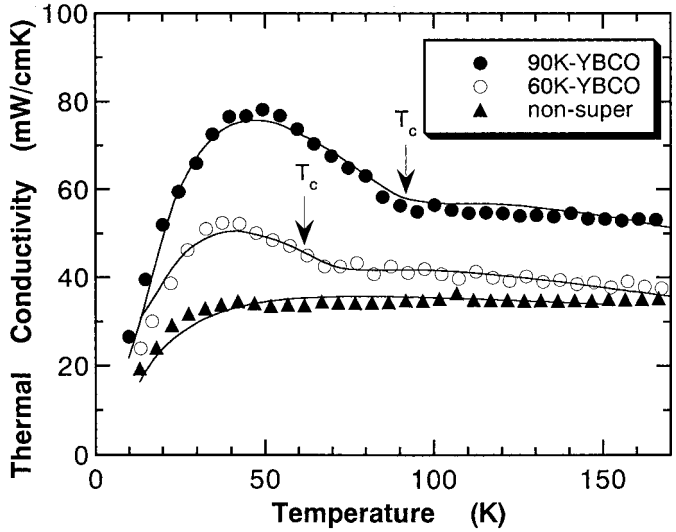

Fig. 2. $\varkappa(T)$ vs. T for 90 K-, 60 K- and non-superconductive YBCO. $\varkappa(T)$ takes a maximum at $T_{max} \approx 45$ K for 90 K-YBCO and at $T_{max} \approx 37$ K for 60 K-YBCO. The solid lines represent the theoretical curves calculated by use of the parameter values in Table 1. d-wave symmetry is assumed for 90 K- and 60 K-YBCO (see text)

Table 1
Fitting parameters for the weak coupling of d- and s-wave symmetry with $\Delta_{max} = \Delta_0 = 1.5\Delta_{BCS}$

	τ_b^{-1} (10^8 s^{-1})	s (10^6 K^{-2} s^{-1})	P (10^3 K^{-4} s^{-1})	E (10^8 K^{-1} s^{-1})	U (10^3 K^{-3} s^{-1})	Θ_D (K)	λ
d-wave							
90 K-YBCO	4.7	3.2	0.23	12	3.6	400	0.42
60 K-YBCO	4.9	3.3	1.2	4.3	3.4	400	0.16
s-wave							
90 K-YBCO	4.6	4.0	0.7	4.7	2.4	400	0.16
60 K-YBCO	4.8	5.0	1.2	3.5	2.7	400	0.13
non-super							
-YBCO	11	5.6	6.4	0	3.0	400	0

creases monotonically with decreasing temperature. The temperature dependence of $\varkappa(T)$ of the non-superconductive sample is very small above $\approx$40 K.

Fig. 3 shows the thermal diffusivity $\alpha(T)$ of 90 K- and 60 K-YBCO as a function of temperature. $\alpha(T)$ of 90 K-YBCO is larger than that of 60 K-YBCO and increases with decreasing temperature. It is noticed that α increases more rapidly below T_c than above T_c. The temperature dependence and the absolute values of $\alpha(T)$ of 90 K-YBCO are consistent with other reports [5, 6]. As for 60 K-YBCO, there are no available other data on $\alpha(T)$ to compare as far as we know.

Since we measured both the thermal conductivity $\varkappa$ and diffusivity α, the specific heat can be determined by use of the relation, $C = \varkappa/\alpha$. Fig. 4 shows the estimated specific heat per mole (C_M) together with typical curves of the Debye specific heat. Neglecting

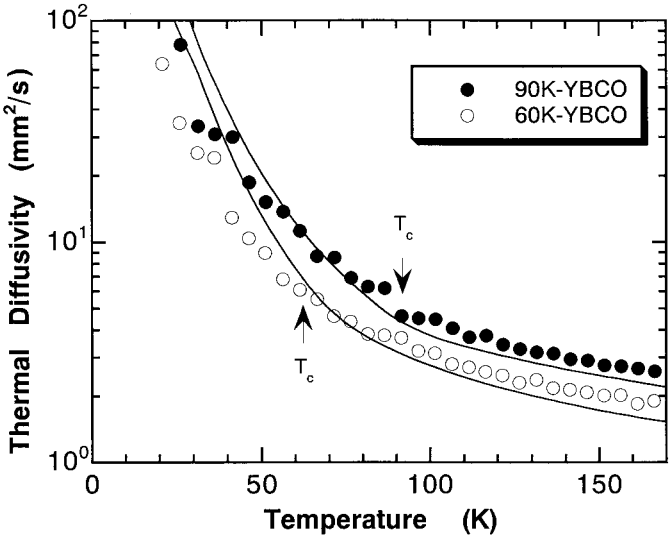

Fig. 3. The thermal diffusivity α vs. T for 90 K- and 60 K-YBCO. The solid lines represent the theoretical curves calculated by use of the parameter values in Table 1. d-wave symmetry is assumed (see text)

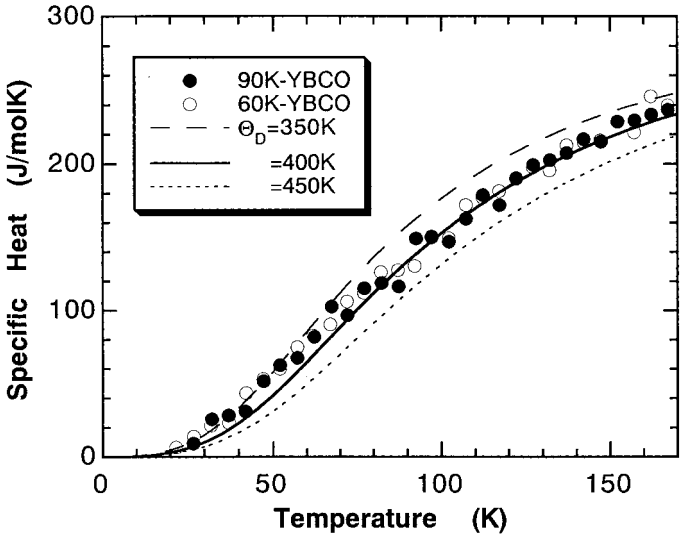

Fig. 4. The specific heat C determined from the relation $C = \varkappa/\alpha$. C vs. T curves of both 90 K- and 60 K-YBCO are consistent with Debye specific heat with $\Theta_D = 400$ K

the electronic contribution C_e to the total specific heat C in this rather low carrier density cuprate system and in this rather high temperature range, the Debye temperature Θ_D of each sample is determined to be 400 K for both 90 K- and 60 K-YBCO from the best fitting Debye curve.

Fig. 5 shows the temperature dependence of the longitudinal sound velocity v_s^L of the present 90 K-, 60 K- and non-superconductive YBCO. The sound velocities of respec-

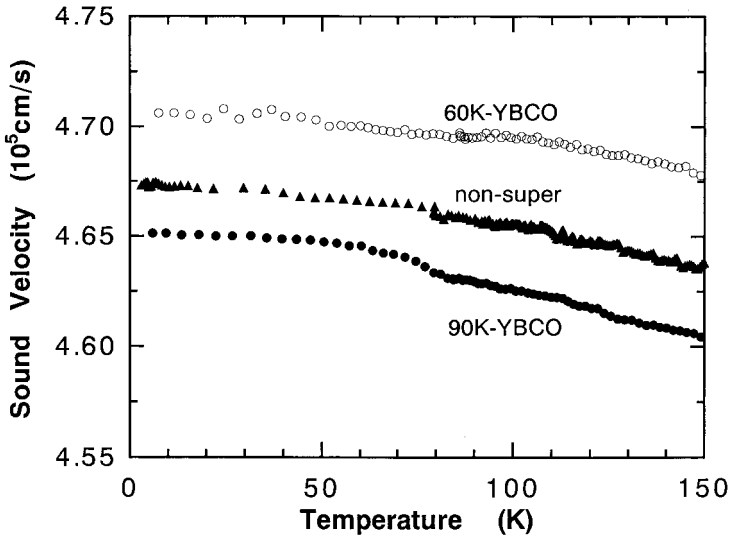

Fig. 5. Velocity $v_s^L(T)$ of longitudinal ultrasound ($\approx$7 MHz) of 90 K-, 60 K- and non-superconductive YBCO

tive samples are roughly the same and no systematic dependence on oxygen deficiency δ is noticeable. This result is consistent with the specific heat data in Fig. 4, where no difference of Θ_D is noted between 90 K- and 60 K-YBCO.

4. Discussion

Similarly to conventional metal and alloy superconductors, both electrons and phonons contribute to the heat conduction also in high-T_c oxides. With decreasing temperature in the superconducting state, more and more electrons (= quasi particles) condense into the Cooper pairs with zero entropy, which do not carry heat nor scatter phonons. Then the number density of quasi particles $n_{qp}(T)$ is a key parameter to determine both the electron thermal conductivity $\varkappa_{es}$ and the phonon thermal conductivity $\varkappa_{phs}$ of a superconductor. In the following sections, we make synthetic analyses on the temperature dependence of $\varkappa_{es}(T)$ and $\varkappa_{phs}(T)$ and try to get information on the energy gap symmetry, which is one of the main topics of current physical interest. In the present analyses we presume the maximum energy gap Δ_{max} to be larger than the BCS gap Δ_{BCS} ($= 1.76 k_B T_c$) because the majority of tunneling [7 to 9] and photo-emission experiments [10 to 12] etc. have supported the larger energy gap values of $2\Delta_{max}/k_B T_c \approx 5$ to 9 of high-T_c cuprates.

4.1 Estimation of the electron thermal conductivity $\varkappa_{es}$ below T_c

In conventional superconductors in which the electron scattering by impurities is dominant, the electron thermal conductivity $\varkappa_{es}(T)$ rapidly decreases relatively to the corresponding normal state component $\varkappa_{en}(T)$ because of rapid reduction of $n_{qp}(T)$ with decreasing temperature. For cuprate superconductors, however, a variety of experimental studies have suggested a drastic suppression [12, 13] of the quasi-particle scattering rate τ_{qp}^{-1} in comparison to the normal state electron scattering rate τ_e^{-1}. Since the electron thermal conductivity is roughly proportional to the product $n_{qp}(T)\,\tau_{qp}(T)$, the enhancement of $\varkappa_{es}$ below T_c is possible if the increase of the quasi-particle scattering time $\tau_{qp}(T)$ overcompensates the decrease of $n_{qp}(T)$ [14 to 17]. Here we estimate $\varkappa_{es}(T)$ in the superconducting state by use of the following formula derived by Kadanoff and Martin [18]:

$$\frac{\varkappa_{es}}{\varkappa_{en}} = \frac{3}{4\pi^2} \int_0^{2\pi} d\varphi \int_0^{\infty} d\varepsilon\, \varepsilon^2 \operatorname{sech}^2 \left\{ \frac{1}{2} [\varepsilon^2 + (\beta\Delta)^2]^{1/2} \right\} \frac{1 + at^n}{\dfrac{\varepsilon}{[\varepsilon^2 + (\beta\Delta)^2]^{1/2}} + at^n}, \qquad (1)$$

where ε is the electron energy relative to the chemical potential, β is $1/k_B T$ and t is the reduced temperature T/T_c. $\varkappa_{en}$ is equal to $(\pi^2/3)\,(n_e/m)\,k_B T \tau_e$ (we assume the Wiedemann-Franz law), m and n_e being the mass and the density of the electron, respectively. The energy gap Δ is assumed to be $\Delta = \Delta_0$ for s-wave coupling, and $\Delta = \Delta_{max} \cos 2\varphi$ for d-wave coupling, φ being the azimuthal angle in the two-dimensional circular Fermi surface. We assume that below T_c the electrical resistivity (i.e., quasi-particle resistivity) follows t^n temperature dependence with the residual resistivity equal to $\varrho(T_c)/(a+1)$ at 0 K,

$$\varrho(T) = \varrho(T_c) \left(\frac{1}{a+1} + \frac{a}{a+1}\, t^n \right), \qquad (2)$$

where $\varrho(T_c)$ is the resistivity value at T_c. In eq. (2) the first term corresponds to the residual resistivity $\varrho(0)$ and the second term stands for the temperature dependent part of the resistivity. The a value in eqs. (1) and (2) is the ratio of the two terms at T_c. For the electrical resistivity above T_c ($t > 1$), n is set to be unity in eq. (2) to be consistent with experimental results. From the linear extrapolation of $\varrho(T)$ lines in Fig. 1, a is estimated to be 1.7 for the 90 K-phase sample and 2.6 for the 60 K-phase sample. Following the results of the tunneling spectroscopy due to Nantoh et al. [7], we take the maximum energy gap value $\Delta_{max} = \Delta_0 = 1.5\Delta_{BCS}$ and calculated eq. (1) for various n values and for both d- and s-wave symmetries. The calculated curves under d-wave energy gap are presented in Fig. 6 for 90 K-YBCO and in Fig. 7 for 60 K-YBCO.

According to our calculation, the d-wave model always resulted in a considerably larger electronic component $\varkappa_{es}$ than the s-wave model below T_c. This is reasonable because more quasi-particles survive at all temperatures below T_c under anisotropic d-wave energy gap and carry heat. In Figs. 6 and 7, it is clearly seen that no enhancement in $\varkappa_{es}$ can be expected near T_{max} ($T_{max} \approx 45$ K for 90 K-YBCO and ≈ 37 K for 60 K-YBCO) even if we assume rather drastic t^6 depression of quasi-particle scattering below T_c and d-wave gap symmetry; $\varkappa_{es}(T_{max})$ is always smaller than or, at most, almost equal to $\varkappa_e(T_c)$. This ceiling of $\varkappa_{es}$ is caused by the sizable residual resistivity $\varrho(0)$ of our 'dirty' YBCO samples. It is plausible that the possible maximum of the quasi-particle thermal conductivity $\varkappa_{es}(T)$ cannot exceed $LT/\varrho(0)$ (L being the Lorentz number), which is given by the linear line crossing the origin in Figs. 6 and 7. At T_{max}, the possible maximum enhancement in $\varkappa_{es}$ measured from $\varkappa_e(T_c)$ ($\Delta\varkappa_{es}^{max}$) is about 2 mW/cm K for 90 K-YBCO and ≈ 4 mW/cm K for 60 K-YBCO. Even these values of $\Delta\varkappa_{es}^{max}$ are

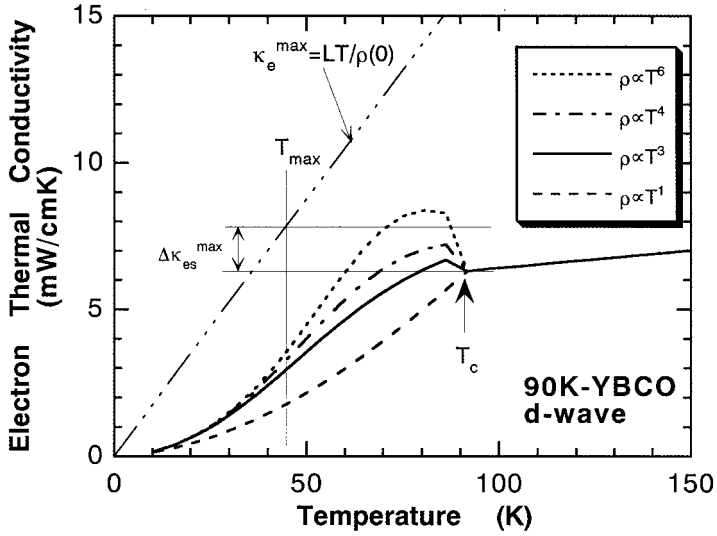

Fig. 6. Estimation of electronic thermal conductivity $\varkappa_{es}$ for 90 K-YBCO. The energy gap is assumed to have d-wave symmetry, $\Delta = 1.5\Delta_{BCS}\cos 2\varphi$. The quasi-particle scattering rate is assumed to have T^n dependence on temperature T. The linear line $LT/\varrho(0)$ (L is the Lorentz number, $\varrho(0) = 1.13$ mΩ cm) represents the possible maximum electronic thermal conductivity. T_{max} is the temperature at which the observed $\varkappa(T)$ takes maximum. $\Delta\varkappa_{es}^{max}$ is the possible maximum enhancement of $\varkappa_{es}$ at T_{max} measured from $\varkappa_e(T_c)$

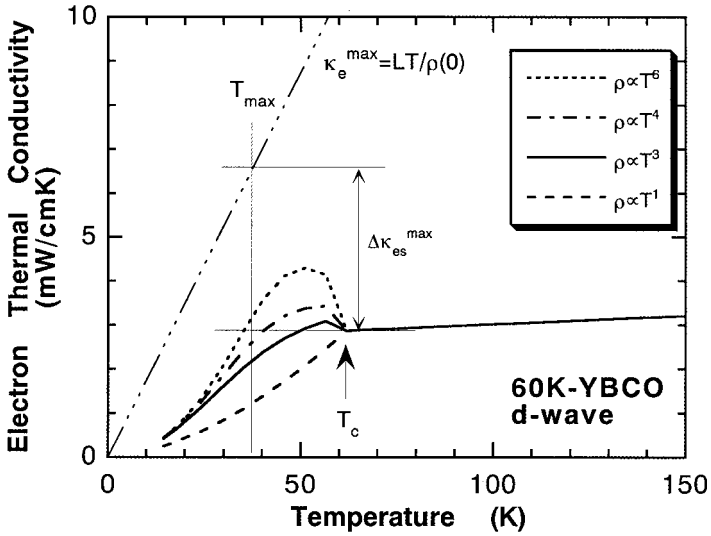

Fig. 7. Estimation of $\varkappa_{es}$ for 60 K-YBCO. d-wave energy gap $\Delta = 1.5\Delta_{BCS}\cos 2\varphi$ is assumed. The line $LT/\varrho(0)$ ($\varrho(0) = 0.14\,\mathrm{m\Omega\,cm}$) represents the possible maximum electronic thermal conductivity. T_{max} is the temperature at which the observed $\varkappa(T)$ takes maximum. $\Delta\varkappa_{es}^{max}$ is the possible maximum enhancement of $\varkappa_{es}$ at T_{max} measured from $\varkappa_e(T_c)$

almost negligibly small compared to the observed enhancement $\Delta\varkappa_{ob} \approx 30$ mW/cm K and $\approx$15 mW/cm K for 90 K and 60 K-YBCO. It is also to be noticed that the present estimation of $\varrho(0)$ by the linear extrapolation to 0 K may be the lower limit because $\varrho(T)$ in the normal state should be deviate upwards from the T-linear line at low temperatures to cross the 0 K ordinate in the right angle. Thus, $\varkappa$ enhancement observed for the present 90 K- and 60 K-YBCO samples cannot be attributed to the electronic component $\varkappa_e$.

Although the $\varkappa$ enhancement in the present 'dirty' $YBa_2Cu_2O_{7-\delta}$ samples cannot be explained by the electronic component model, it is quite possible that $\varkappa_{es}$ also contributes to the $\varkappa$ enhancement in 'pure' ($\varrho(0) \approx 0$) crystals as Yu et al. [14], Krishara et al. [15] and other research groups have pointed out [16, 17]. Krishara et al. [15] measured the thermal Hall conductivity and concluded that about a half of the $\varkappa$ enhancement observed in their 'pure' 90 K-phase $YBa_2Cu_3O_7$ crystal came from the electronic component. Then the remaining half of the $\varkappa$ enhancement in 'pure' specimens should be of phonon origin. The phonon thermal conductivity of the present 'dirty' specimens is to be analyzed in the following section.

4.2 Analyses of the phonon thermal conductivity $\varkappa_{ph}$ based on the BRT-TW theory

Assuming the Debye spectrum of phonons, the phonon thermal conductivity is generally given by the following formula [19]:

$$\varkappa_{ph} = \frac{3dn_0R\langle v_s^2\rangle}{2\pi M}\left(\frac{T}{\Theta_D}\right)^3 \int_0^{2\pi} d\varphi \int_0^{\Theta_D/T} \frac{x^4\,e^x}{(e^x-1)^2}\,\tau_{ph}(x)\,dx\,, \tag{3}$$

where x is the reduced phonon frequency, n_0 $(= 13 - \delta)$ the number of atoms composing $YBa_2Cu_3O_{7-\delta}$, R the gas constant, d the mass density and M is the molar weight. Equation (3) contains integral over φ to treat the d-wave anisotropy in the superconducting state. The phonon scattering rate τ_{ph}^{-1} is assumed to be given by the sum of contributions of various scattering centers [19],

$$\tau_{ph}^{-1} = \tau_b^{-1} + s(Tx)^2 + p(Tx)^4 + E(Tx)\, g(x,\ y) + UT^3x^2 \exp\left(-\frac{\Theta_D}{bT}\right). \tag{4}$$

Here, the parameters τ_b^{-1}, s, p, E and U respresent the phonon scattering strength due to grain boundaries, sheet-like faults, point defects, conduction electrons and other phonons (umklapp process), respectively, and b $(=2.1)$ is a constant which efficiently limits the cut-off frequency of the umklapp process. The function $g(x,\ y) = \tau_{phn}^{e}/T_{phs}^{e}$ stands for the ratio of the phonon scattering times by electrons in the superconducting and normal states, which was first calculated by Bardeen, Rickayzen and Tewordt (BRT) [20] on the basis of the BCS theory. With decreasing temperature, $g(x,\ y)$ promptly decreases in the superconducting state, depending on the magnitude of the energy gap Δ through the parameter $y = \Delta/k_BT$. The decrease of $g(x,\ y)$ results in the increase of $\varkappa_{phs}$ in the superconducting state as was observed in many conventional superconductors [21]. We calculated $\varkappa_{ph}$ on the basis of eqs. (3) and (4) for both the d- and s-wave energy gap symmetries with $\Delta_{max} = \Delta_0 = 1.5\Delta_{BCS}$. For $\varkappa_{es}$, we assumed t^3 dependence for $\varrho(T)$ below T_c, which corresponds to $\varrho(T)$ limited by the spin fluctuation scattering [17]. The calculated $\varkappa_{es}$ was subtracted from experimental $\varkappa$ to determine $\varkappa_{ph}$. This t^3 assumption does hardly influence on the analyses of $\varkappa_{ph}$ because of the estimated relatively small electronic component $\varkappa_{es}$. The grain boundary scattering time τ_b was determined so as to be consistent with the average grain size observed by SEM. The τ_b values hardly influence on the results of the $\varkappa_{ph}$ analyses either, because the boundary scattering is far weak in comparison to other scattering mechanisms in the temperature range of the present measurement. For the values of Θ_D we used 400 K determined from the estimated C_{ph} for 90 K- and 60 K-YBCO. The average phonon velocity $\langle v_s^2\rangle = \{(v_s^L)^2 + 2(v_s^T)^2\}/3$ (v_s^T being the velocity of the transverse wave) was calculated to be 3.5×10^5 cm/s using the value of v_s^L in Fig. 5 and the velocity ratio $v_s^T/v_s^L = 0.58$ measured for another similarly prepared 90 K phase sample. The best fitting calculation curves of the 90 K- and 60 K-samples are shown in Fig. 8a and b for d- and s-wave symmetries, respectively. The parameter values for the fitting curves in Fig. 8a and b are summarized in Table 1. If we assume the s-wave coupling with $\Delta_0 = 1.5\Delta_{BCS}$, however, the peak position of calculated $\varkappa_{ph}$ of 90 K-YBCO appears at a higher temperature than that of experiment observations irrespective of the choice of parameter values. The peak position of $\varkappa_{ph}$ shifts toward higher temperatures with increasing Δ_0 and the s-wave $\varkappa_{ph}$ curve in Fig. 8b is the one which shows the $\varkappa_{ph}$ maximum at the lowest temperature, keeping reasonable allover fitting. A similar difficulty is noticed also for the 60 K-sample in s-wave model. Thus, the real best fitting is possible only for the d-wave coupling model. Here it is somewhat puzzling that the strong coupling model seems to be incompatible with observed $\varkappa(T)$, because then the peak position of $\varkappa(T)$ should again shift toward higher temperatures even for the d-wave model as pointed out by Tewordt and Wölkhausen [22].

According to Tewordt and Wölkhausen (TW) [19], the coefficient E which represents the strength of scattering by electrons is directly proportional to the electron–phonon

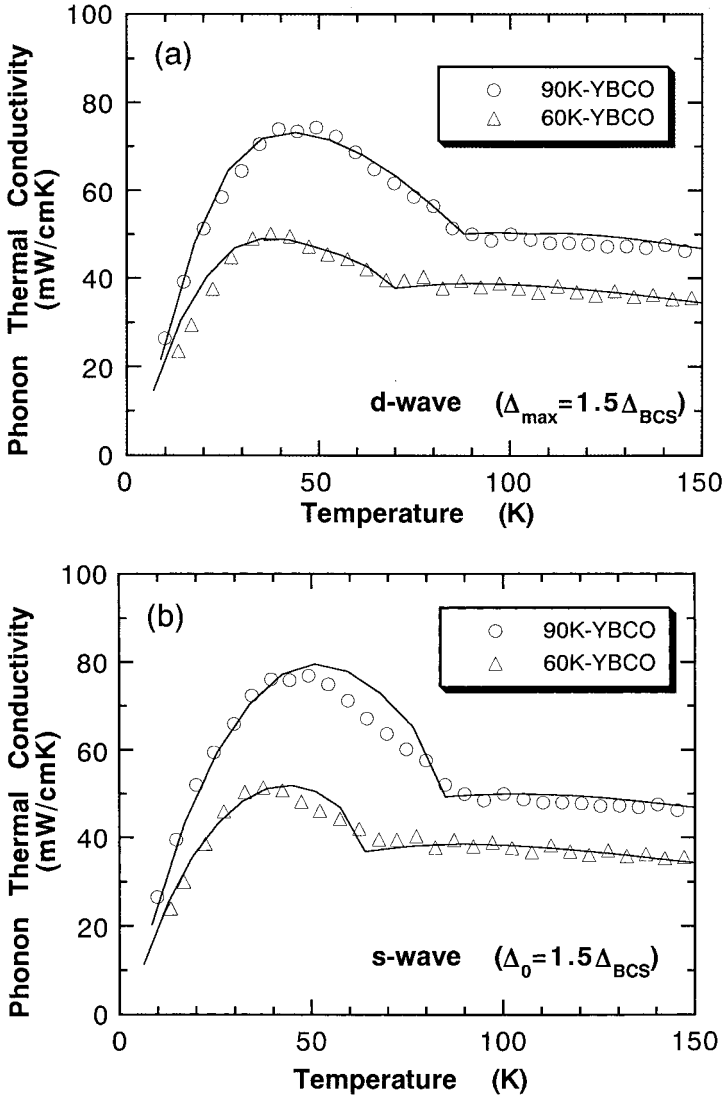

Fig. 8. a) Best fitting curves of phonon thermal conductivity $\varkappa_{ph}$ for 90 K- and 60 K-YBCO. d-wave energy gap $\Delta = 1.5\Delta_{BCS}\cos 2\varphi$ is assumed. The values of parameters used for $\varkappa_{ph}$ calculation are summarized in Table 1. b) Fitting curves for $\varkappa_{ph}$ for 90 K- and 60 K-YBCO. s-wave energy gap $\Delta_0 = 1.5\Delta_{BCS}$ is assumed. The maximum of calculated $\varkappa_{ph}$ occurs at higher temperatures than that of experimental observation irrespective of the choice of parameters values

coupling constant λ through the relation

$$\lambda = \frac{2c\langle t\rangle}{\pi v_s} E, \tag{5}$$

where c is the average lattice constant and $\langle t\rangle$ is the effective hopping matrix element for the two-dimensional electron band. A rough estimation gives $\lambda = 0.42$ for 90 K-

YBCO and $\lambda = 0.16$ for the 60 K-YBCO with values of $c = 4$ Å and $\langle t \rangle = 5000$ K following TW. The estimated values of λ are not so large as to explain such high-T_c values but the electron–phonon interaction is pretty large in the YBCO system and it is noteworthy that the electron–phonon interaction is larger in 90 K-YBCO than in 60 K-YBCO. The contribution of the electron–phonon interaction to superconductivity should not be neglected, though the main origin for the superconductivity of high-T_c cuprates must be attributed to some other mechanisms. As we have pointed out in previous papers [23, 24], the estimated λ values are not much affected by substituting yttrium by other rare-earth elements or by substituting Ba by Sr or Ca atoms.

4.3 Analyses of the thermal diffusivity and the strength of each phonon scattering mechanism

Since the thermal conductivity is given by the sum of the electron component $\varkappa_e$ and the phonon component $\varkappa_{ph}$, we also define the respective components of the diffusivity α as follows:

$$\alpha = \frac{\varkappa}{C} = \frac{\varkappa_{ph}}{C} + \frac{\varkappa_e}{C} = \alpha_{ph} + \alpha_e \,. \tag{6}$$

Since we have already estimated $\varkappa_e$ and $\varkappa_{ph}$ in the preceding section, thus the separation of α_{ph} and α_e is straightforward. If we neglect again the electronic contribution to the specific heat C, α_{ph} is given by

$$\alpha_{ph} \approx \frac{\varkappa_{ph}}{C_{ph}} = \frac{v_s^2}{3} \frac{\int_0^{\Theta_D/T} \tau_{ph}(x) \dfrac{x^4 e^x}{(e^x - 1)^2} \, dx}{\int_0^{\Theta_D/T} \dfrac{x^4 e^x}{(e^x - 1)^2} \, dx} = \frac{v_s^2}{3} \langle \tau_{ph} \rangle = \frac{v_s l_{ph}}{3} \,. \tag{7}$$

Equation (7) defines the average phonon relaxation time $\langle \tau_{ph} \rangle$ over the Debye phonon spectrum. The calculated $\alpha(T)$ using parameters for d-wave symmetry in Table 1 is presented by solid lines in Fig. 3. The calculated curves reproduce the experimental data pretty well except for the lower temperature region, which supports the self-consistency and reliability of our present analyses.

Finally, we discuss the strength of each scattering mechanism operative in the present $YBa_2Cu_3O_{7-\delta}$ samples. Figs. 9a and b show the calculated scattering rate $\langle \tau_{ph} \rangle^{-1}$ which indicates the contributions of various scattering centers. Each curve in Fig. 9 which represents the strength of respective scattering centers was obtained by calculating $\langle \tau'_{ph} \rangle^{-1}$ based on eq. (7) and parameter values in Table 1, assuming that a certain scattering term in eq. (4) was removed, and then by subtracting calculated $\langle \tau'_{ph} \rangle^{-1}$ from the total $\langle \tau_{ph} \rangle^{-1}$. We see that the point defects (pT^4x^4 in eq. (4)) are strong phonon scatters in a very wide temperature range except for very low temperatures. The point defect scattering is stronger in 60 K-YBCO because of abundant oxygen vacancies. Electrons also strongly scatter phonons above T_c in 90 K- and 60 K-YBCO but become ineffective at low temperatures in the superconducting state. Phonon–phonon umklapp scattering becomes important at high temperatures above 100 K. The sheet-like faults (sT^2x^2 due to stacking faults etc.) become efficient scattering centers below about 30 K. The grain boundary scattering is always very small in the temperature range above 15 K.

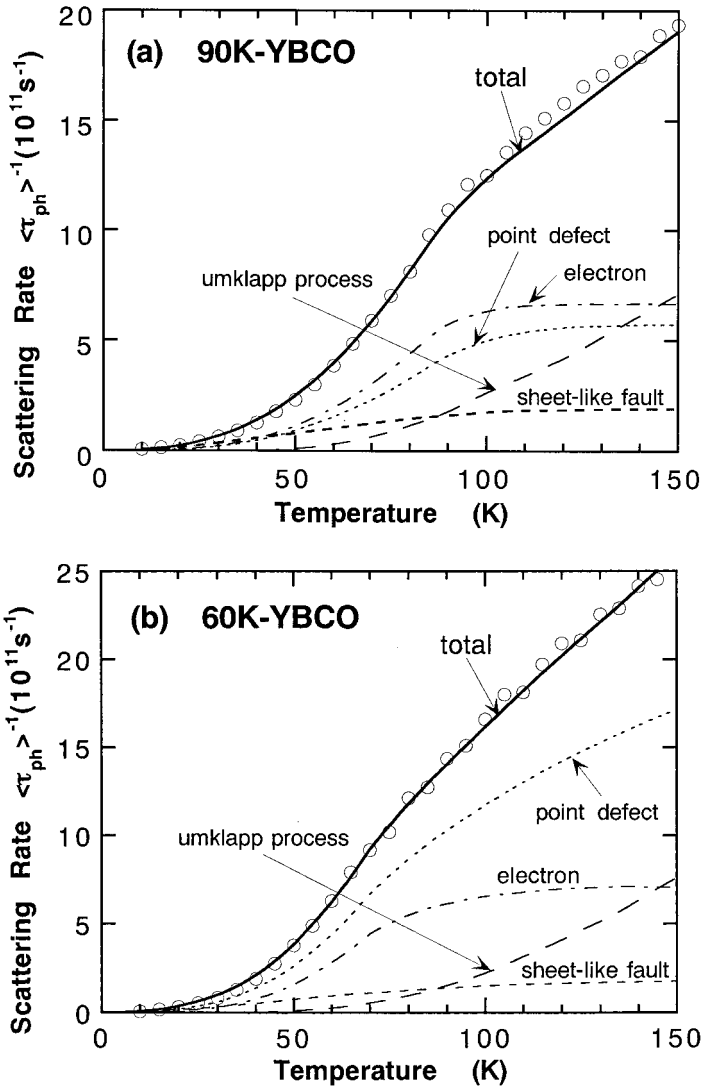

Fig. 9. a) Calculated phonon scattering rate $\langle\tau_{\rm ph}\rangle^{-1}$ for 90 K-YBCO and contributions of each scattering mechanism. The contributions of each scattering mechanism is estimated assuming that the very scattering mechanism is completely removed (see text). Open circles are the experimental points corresponding to the observed thermal conductivity $\varkappa(T)$. d-wave symmetry for the energy gap is assumed and the parameter values of Table 1 are used. b) Calculated phonon scattering rate $\langle\tau_{\rm ph}\rangle^{-1}$ for 60 K-YBCO and contributions of each scattering mechanism. Open circles are the experimental points corresponding to $\varkappa(T)$. d-wave symmetry is assumed

5. Summary

We have measured simultaneously the thermal conductivity $\varkappa$ and the thermal diffusivity α of $YBa_2Cu_3O_{6.90}$ (90 K-phase) with $T_c = 92$ K and $YBa_2Cu_3O_{6.65}$ (60 K-phase)

with $T_c = 62$ K. $\varkappa$ and α have been systematically analyzed. Important conclusions are summarized in the following.

(i) The electronic heat conduction does hardly contribute to the characteristic enhancement of $\varkappa$ below T_c in sintered 'dirty' 90 K- and 60 K-$YBa_2Cu_3O_{7-\delta}$ because of relatively large residual resistivity $\varrho(0)$ in the present samples.

(ii) The observed enhancement of $\varkappa$ below T_c is almost entirely of phonon origin in the present specimens.

(iii) Analyses based on the dominant phonon conduction model support the d-wave-like energy gap anisotropy if we assume the maximum energy gap to be equal to or larger than $\Delta_{max} = 1.5\Delta_{BCS}$.

(iv) The strong coupling model seems to be incompatible with the behavior of observed $\varkappa$ because the effect of the strong coupling is expected to shift peak position of $\varkappa$ to much higher temperatures than experimental results.

(v) Electron–phonon coupling is pretty strong, especially in 90 K-phase YBCO and its contribution to superconductivity should not be neglected.

(vi) Among various scattering mechanisms for phonons, scatterings by electrons and point defects are dominant except in the very low temperature region. The phonon scattering by oxygen vacancies is stronger in $YBa_2Cu_3O_{6.65}$ (60 K-phase) than in $YBa_2Cu_3O_{6.90}$ (90 K-phase).

Acknowledgements The authors wish to thank Dr. M. Kikuchi of Tohoku University for her guidance to the iodometric titration. The contribution to iodometry measurement by Mr. A. Sakamoto of Tohoku University is greatly acknowledged. The sound velocity measurement and iodometry were performed under the inter-university cooperative research program of the Institute for Materials Research, Tohoku University.

References

[1] M. Ikebe, H. Fujishiro, T. Naito, and K. Noto, J. Phys. Soc. Jpn. **63**, 3107 (1994).
[2] H. Fujishiro, T. Naito, M. Ikebe, and K. Noto, Cryogenic Engng. **28**, 582 (1993) (in Japanese).
[3] M. Grtvitch and A. T. Fiory, Phys. Rev. Lett. **59**, 1337 (1987).
[4] K. Takenaka, K. Mizuhashi, H. Takagi, and S. Uchida, Phys. Rev. B **50**, 6534 (1994).
Y. Nakamura and S. Uchida, Phys. Rev. B **47**, 8369 (1993).
[5] T. Higashi, M. Ohnuki, S. Ishi, H. Kubota, and T. Fujiyoshi, Physica **185/189C**, 1357 (1991).
[6] J. Issac, J. Phillip, and B. K. Chaudhuri, Pramāna–J. Phys. **32**, L167 (1989).
[7] M. Nantoh, T. Hasegawa, W. Yamaguchi, A. Takagi, M. Ogino, and K. Kikuchi, J. Appl. Phys. **75**, 5227 (1994).
[8] C. Manabe, M. Oda, and M. Ido, Physica **235/240C**, 797 (1994).
[9] Ch. Renner and F. Fisher, Phys. Rev. B **51**, 9208 (1995).
[10] Z.-X. Shen, D. S. Dessau, B. O. Wells, D. M. King, W. W. Spicer, A. J. Arko, D. Marshall, L. W. Lombardo, A. Kapitulnik, P. Dickinson, S. Doniach, J. DiCarlo, A. G. Loeser, and C. H. Park, Phys. Rev. Lett. **70**, 1553 (1993).
[11] T. Yokoya, T. Takahashi, T. Mochiku, and K. Kadowaki, Phys. Rev. B **53**, 2579 (1996).
[12] D. B. Ronoro, C. D. Porter, D. B. Tanner, L. Forro, D. Mandrus, L. Mihaly, G. L. Carr, and G. P. Williams, Phys. Rev. Lett. **68**, 1590 (1992).
[13] D. A. Bonn, R. Ling, T. M. Riseman, D. J. Baar, D. C. Morgan, K. Zhang, P. Dosanjh, T. L. Duty, A. MacFarlane, G. D. Morris, J. H. Brewer, and W. N. Hardy, Phys. Rev. B **47**, 11314 (1993).
[14] R. C. Yu, M. B. Salamon, J. P. Harris, and N. P. Ong, Phys. Rev. Lett. **69**, 1431 (1992).
[15] K. Krishara, J. M. Harris, and N. P. Ong, Phys. Rev. Lett. **75**, 3529 (1995).

[16] M. HOUSSA, M. AUSLOOS, and S. SERGENKOV, J. Phys.: Condensed Matter **8**, 2043 (1996).
[17] P. J. HIRSCHFELD and W. O. PUTTIKA, Phys. Rev. Lett. **77**, 3909 (1996).
[18] L. P. KADANOFF and P. C. MARTIN, Phys. Rev. **124**, 670 (1962).
[19] L. TEWORDT and T. WÖLKHAUSEN, Solid State Commun. **70**, 839 (1989).
[20] J. BARDEEN, G. RICKAYZEN, and L. TEWORDT, Phys. Rev. **113**, 982 (1959).
[21] M. IKEBE, T. NAITO, H. FUJISHIRO, K. NOTO, N. KOBAYASHI, and K. MORI, Physica **219/220B**, 80 (1996).
[22] L. TEWORDT and T. WÖLKHAUSEN, Solid State Commun. **75**, 515 (1990).
[23] M. IKEBE, H. FUJISHIRO, K. NAKASATO, and K. NOTO, Physica **263C**, 309 (1996).
[24] H. FUJISHIRO, K. NAKASATO, S. TAKAHASHI, and M. IKEBE, Czech. J. Phys., Suppl. **46**, 1207 (1996).